Non-peer-reviewed preprint submitted to EarthArXiv

The Bhote Koshi–Trishuli flash flood of 26 August 2026, Rasuwa, Nepal: warning latency exceeded flood travel time

Sunim Acharya
Independent researcher, San Francisco, California, United States
Correspondence: sunim.54@gmail.com
ORCID: https://orcid.org/0009-0003-1207-3610

Status. This is a non-peer-reviewed preprint submitted to EarthArXiv. This manuscript has not been submitted to a journal for peer review at the time of posting. Any subsequent submission, and the resulting journal DOI, will be recorded in a revised version of this preprint.

Data and code. The validated data package and the analysis that produces every figure and table in this paper are archived at https://doi.org/10.5281/zenodo.22153581 under CC-BY-4.0.

Note on provisional figures. Casualty totals for this event were still being revised by the responsible agencies when this version was prepared. The figures used are dated in the text and in the archived data package, and the analysis depends on the spatial distribution of recoveries rather than on the totals.

The Bhote Koshi–Trishuli flash flood of 26 August 2026, Rasuwa, Nepal: warning latency exceeded flood travel time

Sunim Acharya[1]

[1]Independent researcher, San Francisco, California, United States

Correspondence: Sunim Acharya (sunim.54@gmail.com)

Abstract. An ice–rock mass detached from the northern flank of the Langtang massif, Nepal, at 08:37:10 Nepal Time on 26 August 2026, blocked the Lhende Khola and released a cascade that killed more than 500 people along the Bhote Koshi–Trishuli–Narayani corridor. This study measures the warning chain end to end, combining the reviewed seismic origin time with the gauge chronology published by Nepal's Flood Forecasting Division. The mass public alert followed the trigger by 38.8 min while the wave reached the first inhabited gauge in 12.8 min, giving a lead time of -26 min there and -6 to $+4$ min at the next settlement downstream. The two uppermost destroyed gauges were lost at 27 % and 87 % of their own warning stages, so threshold logic never fired. Fatalities concentrated in the two districts where lead time was negative or negligible, while districts warned hours in advance became the body-recovery zone. A closed-form energy budget excludes frictional meltwater as the flood's source, because supplying the measured 19.96×10^6 m^3 excess volume would require melting four times the ice in the entire 2021 Chamoli detachment. The constraint on survival was the time the institutional chain consumed, not flood magnitude.

1 Introduction

High-mountain Asia supplies water to roughly a quarter of the world's population from a cryosphere in rapid retreat (Immerzeel et al., 2020), and it is producing large ice–rock detachments faster than warning systems are being adapted. The 2016 Aru twin collapses (Kääb et al., 2018), the 2021 Chamoli disaster (Shugar et al., 2021) and recurrent Sedongpu failures on the Yarlung Tsangpo (Li et al., 2022) established that glacierised bedrock slopes can fail at 10^7–10^8 m^3 with little warning, and more often than was assumed (Kääb et al., 2021). Glacier thinning, rising equilibrium line altitudes and warming of the frozen bedrock bond in steep faces are documented and accelerating (Gruber and Haeberli, 2007; Hugonnet et al., 2021; Maurer et al., 2019).

Most hazard research addresses where the next failure will occur and how far the resulting flow will travel. A third question determines whether people live: once a cascade has started, how much of its travel time becomes usable warning? Sättele et al. (2015) formalised early-warning reliability as a chain in which detection, transmission and response each consume time, and Cook et al. (2021) demonstrated the detection half of that chain for Chamoli, showing that regional seismic networks resolved the flow at ranges up to 100 km and could in principle have supported downstream warning. What remains scarce is measurement of the realised chain, end to end, against a fatal event, because the necessary combination is seldom available. It requires an instrumentally constrained trigger time together with a documented downstream arrival chronology.

The 26 August 2026 Bhote Koshi–Trishuli disaster supplies that combination, on a massif with a recent and fatal mass-movement record: the 2015 Gorkha earthquake triggered an avalanche into Langtang village that killed more than 200 people, its runout amplified by anomalous winter snow (Fujita et al., 2017). The trigger has a reviewed seismic origin time, and Nepal's Flood Forecasting Division published a minute-resolution chronology of gauge failures, bulletin issuance and downstream arrivals. The flow travelled about 190 km of channel through a population whose exposure was broadly comparable along the corridor, while the available lead time varied by two orders of magnitude, so the corridor behaves as a natural experiment on lead time. The analysis is possible only because Nepal's Department of Hydrology and Meteorology (DHM) released a detailed technical situation report within a day of the event, while the emergency response was still under way. That report closes by recommending a technical review of the forecasting and early warning system, and specifically an analysis of the difference between the observed stage record and the preliminary forecasts. This paper is offered as a contribution to that review.

What follows is an assessment of an architecture rather than of the people who operated it. The limits identified here follow from where the instruments sit and how the decision path is wired, and they would constrain any downstream-gauge network in a catchment of this steepness. Staff acted on the information their instruments provided, and the notification that began the alert sequence came from a district office and from station staff whose own gauge was destroyed twenty minutes later. This paper measures the warning chain and does not simulate the flow, which is not yet supportable, as Sect. 5 sets out. The analysis rests only on open, citable observations.

2 Event and data

At 08:37:10 Nepal Time (NPT, UTC+05:45) on 26 August 2026 a combined ice and bedrock mass detached from the glaciated northern flank of the Langtang massif. The USGS reviewed catalogue (U.S. Geological Survey, 2026) lists the resulting signal as event `us7000tbwb`, M 5.2, at zero depth and event type `landslide`, and a second, smaller failure at the same location followed at 11:45:35 NPT as `us7000tc90`, M 4.2, also typed `landslide`. The GFZ reviewed solution (GFZ Helmholtz Centre for Geosciences, 2026) independently gives M_w 5.7 at the same origin and also types the event a landslide. Both are fixed-depth solutions on different magnitude scales, so neither constrains the mechanism beyond the event type each assigns, and the agreement on that type is what carries weight. Nepal's chronology logs the trigger instead as an M 4.4 earthquake attributed to the Department of Mines and Geology, which was the solution available domestically at the time. For roughly the first half hour, responders were therefore working from a tectonic interpretation, not from a mass movement with an inevitable downstream flood consequence. Distinguishing the two in real time is not routinely possible anywhere, and the reclassification followed later.

Four independent estimates of the initiation point agree within 3.5 km, and every one places the detachment inside Rasuwa district, 3.3 to 6.6 km south of the Nepal–China boundary (Table 1, Fig. 1). The flow path, by contrast, is transboundary, because the Lhende Khola drains north across the border, joins the Bhote Koshi in Gyirong County, Tibet Autonomous Region, China, and the combined flow re-enters Nepal at the Rasuwagadhi crossing. The source lies within Nepal's own jurisdiction; the blockage and the lake it impounded do not. Everything else about the source is contested, and Table 1 carries the reported values without resolving them. Volume is the one that matters here, and the figure in circulation describes the total mass mobilised along the runout, most of it channel and valley fill containing no glacier ice, so it sets no ice budget. Section 3.4 instead adopts a detachment volume bracketing the largest documented Himalayan bedrock–ice failures, and reports how the conclusion behaves if the detached mass were far larger. Expert assessments issued in the days after the event state that no pre-existing glacial lake drained, so the cascade was not a glacial lake outburst flood (ICIMOD, 2026; USGS, 2026).

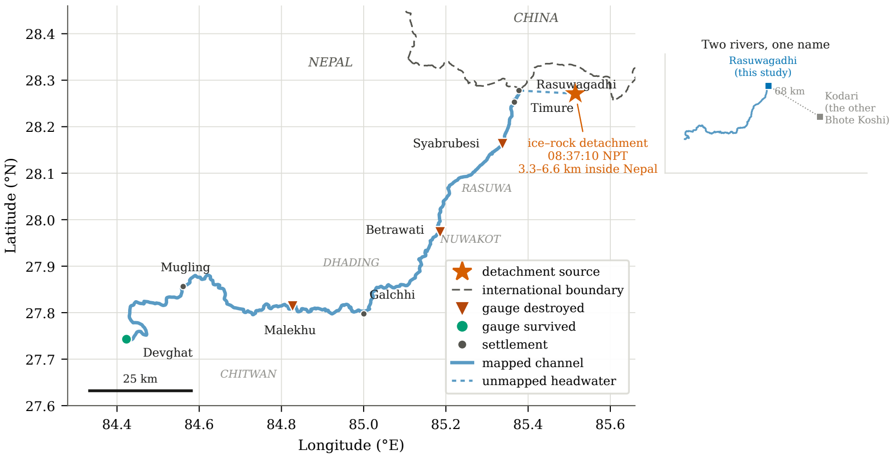

Figure 1. Study area, from OpenStreetMap channel and boundary data. The star marks the detachment source, 3.3 to 6.6 km inside Nepal, and the dashed segment the unmapped headwater reach, carried as a 13.5 to 15.4 km range. Triangles are gauging stations destroyed on 26 August, circles those that survived. The inset distinguishes the two Nepali rivers named Bhote Koshi.

Table 1. Source and corridor parameters as reported, and the values used here. Reported source geometry disagrees between assessments made in the days after the event, and that disagreement is carried through, not averaged away.

Quantity	As reported	Used here
Initiation point	four estimates within 3.5 km	seismic solution
Position vs border	3.3 to 6.6 km south	inside Nepal
Detachment elevation	about 4880 m, or 5200 to 5400 m	not used
Vertical drop	about 1200 m, or about 1830 m	carried as a range
Mobilised volume	more than 10^8 m^3, incl. entrainment	sets no ice budget
Detachment volume	not measured	10 to 30 $\times$ 10^6 m^3
Rasuwagadhi to Devghat	about 168 km (DHM)	178 km measured
Source to Rasuwagadhi	unmapped	13.5 to 15.4 km
Reach sinuosity	not reported	1.09 upper, 1.81 lower
Node to channel	–	within 0.6 km

The propagation record is the technical situation report issued by DHM's Flood Forecasting Division on the day, which gives a minute-resolution chronology, the official warning and danger thresholds at each station, and a discharge analysis at Devghat. Channel distances are measured along the OpenStreetMap river centreline by shortest path (OpenStreetMap contributors, 2026). Sinuosity varies enough between the upper gorge and the lower Narayani that a single corridor-wide value would misstate the lower reaches, so each reach is measured separately. Only the headwater segment above Rasuwagadhi is unmapped, and it is carried throughout as a range, bounded below by the great-circle separation and above by the largest sinuosity measured on the adjacent reaches. Two names require care. Devighat hydropower station in Nuwakot, one of the damaged installations, is not Devghat in Chitwan and Tanahun, the downstream gauge used here. More consequentially for the literature, two Nepali rivers are named Bhote Koshi: the corridor studied here, which drains via Rasuwagadhi to the Trishuli and Narayani in the Gandaki basin, and a second river 68 km east draining via Kodari to the Sun Koshi. The historical outburst record discussed in Sect. 3.5 belongs to the second of these.

3 Results

3.1 The lead-time budget

In the chronology of Table 2, institutional latency, defined as the interval from the physical trigger to the mass public alert, was 38.8 min, while the wave reached the first inhabited monitoring point in 12.8 min. That budget divides into three physically distinct segments. The first ended when the wave reached the gauge, and no domestic architecture could have detected the event before then by observing the river. A further 10.0 min passed between the loss of Syabrubesi telemetry at 08:50 and notification of the Division at 09:00, which is the interval required to recognise a negative signal. The final 16.0 min, from notification to mass dispatch, is confirmation and administrative escalation. Faster procedures can shorten only the last two segments, because the first shrinks only if detection moves from the river to the source.

Lead time at Syabrubesi was -26 min, and at Betrawati the last reading of 3.55 m at 09:20 was already elevated, so the front arrived before that time, and on the station's apparent ten-minute reporting cycle arrival lies between 09:10 and 09:20 with lead time between -6 and $+4$ min. Both settlements in the districts that recorded fatalities therefore had lead time at or below zero within observational uncertainty, while downstream of Betrawati it exceeded one hour everywhere. The alert itself was substantial in reach, but dispatch time is an upper bound on warning performance, because delivery, receipt and response times are not recorded. Under any response-time floor of the kind Sättele et al. (2015) treat as part of the chain, a lead time of a few minutes is not operationally useful, so the negative lead times reported here are conservative. The delay had two structural causes, the first being that the architecture is triggered by downstream gauges, so the first domestic indication was the loss of Syabrubesi telemetry, a negative signal that must be distinguished from ordinary equipment failure before it can be acted on. The escalation path then ran from a district office through the national disaster authority to the meteorological department with no machine-to-machine link, and no arrangement existed for automatic notification across the border, so no upstream signal was available to shorten the interval.

Table 2. Chronology of the 26 August 2026 cascade. Times are NPT. Sources: USGS FDSN event web service for the seismic entries, and the DHM Flood Forecasting Division technical situation report for all others.

Time (NPT)	Δt	Event
08:37:10	0	Detachment, USGS `us7000tbwb`, M 5.2, type `landslide`
08:40	+2.8 min	Syabrubesi gauge, last transmission, 1.62 m
08:50	+12.8 min	Syabrubesi gauge destroyed, telemetry ceases
09:00	+22.8 min	District office and Betrawati station staff notify the Division
09:15	+37.8 min	Confirmation, first early warning issued
09:16	+38.8 min	Mass SMS dispatch, 679 295 messages to four districts
09:20	+42.8 min	Betrawati gauge destroyed, last reading 3.55 m
11:26	+168.8 min	Phurke (Malekhu) gauge crosses its warning level
11:43	+185.8 min	Phurke station and adjacent bridge swept away
11:45:35	+188.4 min	Second detachment at the source, `us7000tc90`, M 4.2
16:00	+442.8 min	Devghat peak, 6.57 m, 5850 $m^3\ s^{-1}$

This gives the architecture a blind zone that no procedure can remove. A downstream-gauge architecture cannot warn any settlement upstream of its first gauge, and can warn those below it only by the margin between wave travel time and institutional latency. Reach-integrated celerity over the reach from the source to Syabrubesi was about 38 m s^{-1}, so that margin was negative along the entire inhabited upper corridor. Celerity then decays monotonically by about a factor of nine to 4.0 m s^{-1} between Mugling and Devghat (Fig. 2), which is the kinematic signature of a hyperconcentrated debris flow relaxing into a flood wave, and the upper-reach value exceeds what was measured at comparable range at Chamoli (Shugar et al., 2021). That estimate rests on reading the 08:50 telemetry cessation as the arrival time. The station reported a normal stage at 08:40, so the front arrived within that ten-minute window, and the earliest admissible arrival would imply celerities an order of magnitude beyond any documented mass flow. Arrival close to 08:50 is therefore the physically consistent reading, and the value used here a conservative one. On any admissible reading the wave reached Syabrubesi well before confirmation. An independent rapid reconstruction of this event recovers about 37 m s^{-1} in the headwater reach from trimline superelevation on opposing valley walls (geo-pera, 2026), a method that shares no input with the arrival-time chronology used here and arrives at the same figure.

Table 3 evaluates four alert architectures against the observed arrivals, and each assumed latency is stated as an assumption. Architecture B assumes an in-channel sensor at the border reporting within 5 min of the wave reaching it. Architectures C and D assume source-side seismic detection with automated dissemination in 5 min and 2 min respectively. Both budgets are consistent with operational debris-flow alarm systems, which achieve detection-to-alarm intervals of order one minute in instrumented catchments (Badoux et al., 2009), and with the demonstrated capability of regional seismic networks to detect and locate flow events of this size within minutes (Cook et al., 2021). Landslides of this magnitude radiate long-period signals whose force histories can be inverted from distant stations (Ekström and Stark, 2013), so the signal that a detector would act on is well characterised. Nepal's national network lies within about 100 km of the source, the range at which Cook et al. (2021)

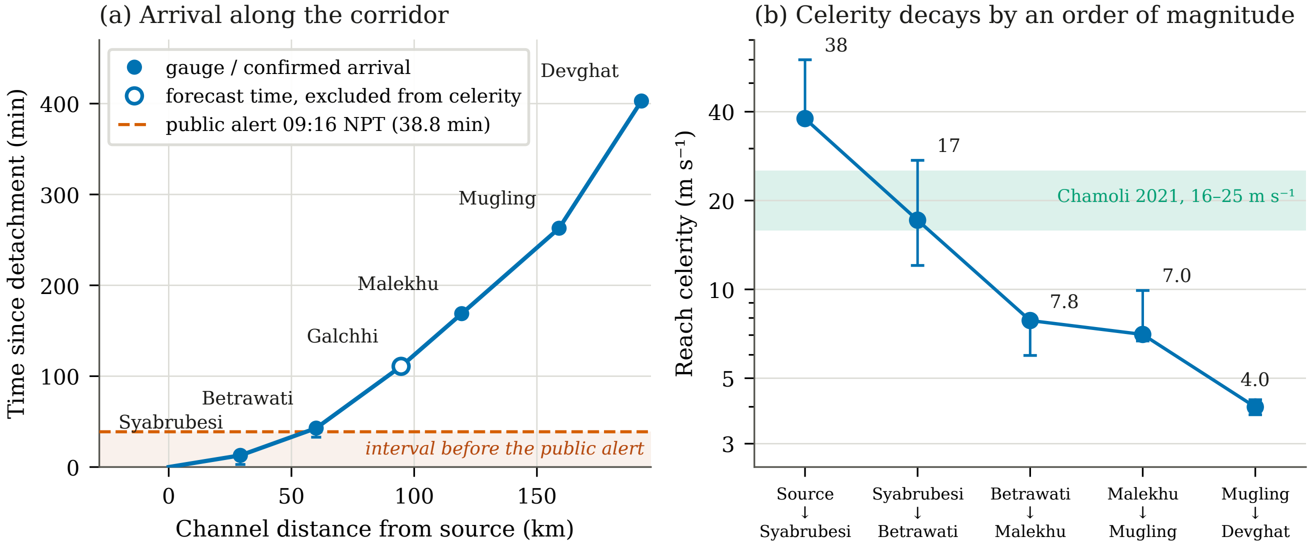

Figure 2. Propagation of the flood wave. (a) Arrival time against measured channel distance from the source. Filled markers are gauge or agency-confirmed observations, the open marker at Galchhi a forecast time excluded from the celerity estimates. Horizontal bars give the headwater distance range and vertical bars the arrival brackets set by station reporting cycles. The dashed line marks the mass public alert. (b) Reach-integrated celerity, decaying by about a factor of nine. The band shows velocities measured at Chamoli 2021 at comparable range (Shugar et al., 2021).

resolved the Chamoli event. Source-side detection is the only architecture tested that moves the first inhabited settlement across zero. Propagating the Syabrubesi arrival bracket, architecture C yields between −2 and +8 min there, so the gain at the uppermost settlement is real but not assured, whereas the gains further downstream of about 34 min at every settlement below Betrawati do not depend on that bracket. Neither architecture protects Timure or Rasuwagadhi, which lie 17 to 19 km of channel from the source. For settlements within roughly ten minutes of travel time from a credible detachment source, the available instrument is siting.

Table 3. Warning lead time in minutes by settlement under four alert architectures. Negative values indicate that the wave arrived before the alert. Architecture A is observed, while B, C and D are counterfactual with the assumed alert latencies stated in the text.

Architecture	Syabru.	Betra.	Galchhi	Malekhu	Mugling	Devghat
A observed	−26	+4	+72	+130	+224	+364
B border sensor	−2	+28	+96	+154	+248	+388
C seismic, 5 min	+8	+38	+106	+164	+258	+398
D seismic, 2 min	+11	+41	+109	+167	+261	+401

3.2 The uppermost gauges were destroyed below their own thresholds

Latency accounts for only half of the failure. Table 4 sets the last recorded stage at each in-path station against that station's official warning and danger levels. The two uppermost destroyed gauges never registered the event. Syabrubesi was lost while reading 27 % of its warning stage and Betrawati at 87 % of its, so a threshold-triggered system would have issued nothing from either. The wave arrived faster than the sampling interval could resolve a rise, and the gauges passed from normal to destroyed without an intervening alarm state. Furthest downstream, Devghat peaked at 6.57 m against a 7.3 m warning threshold, so the station that survived, in the reach with hours of warning, also never crossed its trigger.

Table 4. Last recorded stage at each in-path station against official DHM thresholds. Four stations were destroyed in total, and the fourth, Rasuwa Bhote Koshi, has no published threshold record and is omitted.

Station	Last (m)	Warn (m)	Frac.	Outcome
Bhote Koshi at Syabrubesi	1.62	6.0	0.27	destroyed, never triggered
Trishuli at Betrawati	3.55	4.1	0.87	destroyed, never triggered
Trishuli at Phurke (Malekhu)	10.48	7.0	1.50	triggered 11:26, swept 11:43
Trishuli at Kali Khola	12.3	10.8	1.14	triggered 14:14, survived
Narayani at Devghat	6.57	7.3	0.90	never triggered, survived

Destruction of monitoring infrastructure by the event it is meant to observe is itself a documented failure mode in this region, most directly at Melamchi in 2021, where the Nakote station recorded the flood and was then lost (Maharjan et al., 2021). What the present record adds is the quantified fraction of the station's own threshold at the moment of loss. A gauge destroyed after crossing its threshold has already discharged its warning function, whereas one destroyed at 27 % of threshold never entered the alarm logic at all. The monitoring requirement also does not end with the first failure, because a second detachment from the same source occurred at 11:45:35 NPT, minutes after the Phurke station and its adjacent bridge were swept away, so the source was still producing failures well inside the response window. In a corridor where the wave outruns the gauge network, stage thresholds are the wrong detection variable. The only quantity that rose fast enough to be diagnostic was the loss of telemetry itself. Treating simultaneous telemetry loss at two or more consecutive upstream stations within minutes as a positive alarm condition, and no longer as an equipment fault to be investigated, is a cheap and immediate improvement. Its false-alarm rate is that of concurrent independent telemetry failures, orders of magnitude below that of single-station loss, though the coincidence window requires operational tuning.

3.3 Mortality follows lead time, body recovery does not

Reported fatalities concentrated in Rasuwa and Nuwakot, the reach where lead time was negative or negligible. Copernicus EMS grading of post-event imagery (Copernicus Emergency Management Service, 2026) records 323 buildings destroyed at Syabrubesi and 372 at Timure, both above the confluence, and 1826 at Bidur on the Trishuli, with 2521 destroyed and

3207 graded as affected across the three areas mapped so far. A community of about 250 households in Rasuwa was reported destroyed in its entirety. The service classifies the imaged deposit as a mass movement, not as a flood, at every one of the three sites. Downstream, where lead time exceeded an hour, the wave still arrived with destructive force, reaching 12.3 m at Kali Khola and destroying the Phurke bridge, yet those districts contributed few deaths. The spatial basis of this claim requires care. No dataset of deaths by district of occurrence exists for this event, and the available district-resolved figure is bodies recovered, which is a recovery location and not a mortality location. Infrastructure supplies the check that mortality cannot, because a bridge cannot be carried downstream and counted somewhere else. Of 39 bridges surveyed along the corridor (Humanitarian OpenStreetMap Team, 2026), every one of the 16 in Rasuwa was washed out, against 11 of 13 in Nuwakot, 5 of 7 in Dhading and none of the 3 in Gorkha. That gradient runs the same way as lead time and the opposite way to body recovery, which is what the two measures should do if impact was upstream and retrieval downstream. Mortality location is therefore inferred from where people were swept away, using that gradient, building-destruction counts, the destroyed resettlement community and agency statements, none of which is a mortality census. The inference is reported at that strength.

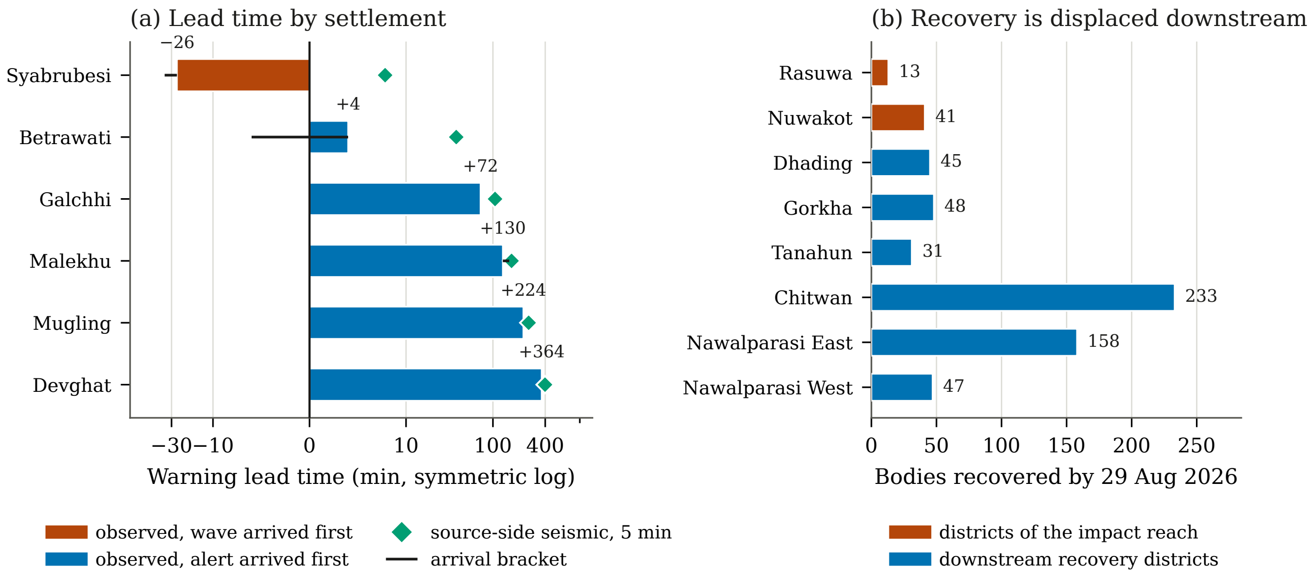

Figure 3. Lead time and its consequences. (a) Warning lead time at each settlement under the observed architecture, shown as bars, and under source-side seismic detection with a five-minute budget to public message, shown as diamonds, on a symmetric-log axis. Horizontal lines are arrival brackets. (b) Bodies recovered by district as of 29 August 2026, ordered downstream.

Recovery displaced downstream by 100 to 250 km. Totals were still rising through the compilation of this study, from 538 dead and 977 missing reported by NDRRMA at 15:00 NPT on 28 August to 616 and 1924 on the following morning, and the spatial distribution held its shape throughout. Of bodies recovered, 233 were in Chitwan and 158 in Nawalparasi East against 13 in Rasuwa (Fig. 3b), with 121 taken from the Narayani alone. The persistence of that shape is itself informative, because the total rose by a quarter over the day while the Rasuwa count did not move at all, so the downstream displacement of recovery widens with time since the event. Only aggregate counts are used here, and no named missing-person registries were ingested. District mortuary capacity was exceeded roughly five- to eightfold in the districts that received the bodies. Hospital morgues in Chitwan hold 30 to 50 and an emergency facility for about 250 was required, while Kaski's combined capacity of 88 received 93 bodies transported from four other districts. This spatial decoupling of mortality from recovery appears not to have been quantified previously in the cascading-hazard literature, and it carries a direct operational consequence. For long-runout mountain cascades, mortuary and disaster-victim-identification capacity requires planning at basin scale rather than district scale, and search effort requires allocation to reaches that an impact model would not identify as affected.

3.4 The frictional melt budget

Early commentary on this event raised the possibility that the energy of the fall melted the detached ice and that the meltwater became the flood. The proposition is testable in closed form, and two partitions of the frictional heat bracket the physics. Under a mass-proportional partition, each kilogram of the falling mass converts its own potential energy to heat where that heat is generated, so ice melts only from dissipation within the ice fraction, and the melt fraction f of the ice mass is

$$f = \frac{gH}{L_\mathrm{f} + c_\mathrm{i}\,\Delta T}, \qquad (1)$$

where g is gravitational acceleration, H the vertical drop, $L_\mathrm{f} = 3.34 \times 10^5$ J kg^{-1} the latent heat of fusion, $c_\mathrm{i} = 2100$ J kg^{-1} K^{-1} the specific heat capacity of ice and ΔT its initial temperature below freezing. For $H = 1200$ to 1830 m and ice initially between 0 and $-10\,^\circ$C, Eq. (1) gives $f = 3.3$ to 5.4 %. Under an all-to-ice partition, every joule of the total mass's potential energy reaches the ice, with none lost to rock heating, comminution, air drag, acoustic radiation or the substrate, and the melt is capped by the ice actually present. The second is a strict thermodynamic ceiling rather than a physical expectation, and Chamoli shows that it can be approached, because frictional heating there melted nearly all of the ice in an 80:20 rock-to-ice mass (Shugar et al., 2021), which under this formulation requires roughly 70 % of the total potential energy to have reached the ice over the full runout drop. The flood volume is measured independently at Devghat. DHM computed a peak discharge of 5850 m^3 s^{-1} at 16:00 against a base flow of 2600 m^3 s^{-1}, giving 57.40×10^6 m^3 of total flow and an excess flood volume of 19.96×10^6 m^3. These are rating-curve quantities derived from stage during a sediment-laden flood with four upstream stations destroyed, and hyperconcentrated flow and event-scale channel change can shift such a rating by tens of per cent. The conclusion below is insensitive to that uncertainty, as the margins show.

For detachments of 10 to 30×10^6 m^3 at ice fractions of 0.2 to 0.5, frictional melt yields 0.06 to 0.74×10^6 m^3 under the mass-proportional partition, which is 0.3 to 3.7 % of the flood, and 0.62 to 3.78×10^6 m^3 at the thermodynamic ceiling, which is 3.1 to 18.9 % (Fig. 4a). The inverse statement is stronger because it needs no assumption about the heat partition at all. Supplying 19.96×10^6 m^3 of water requires melting 21.8×10^6 m^3 of ice completely, and the entire Chamoli 2021 detachment contained about 5.4×10^6 m^3 of ice, being 27×10^6 m^3 at 20 % ice by volume, so the requirement is four times that, with every gram melted and none surviving into the deposit. Complete melting would match the flood only at bulk detachment volumes of 44 to 109 × 10^6 m^3 for ice fractions of 0.5 to 0.2. Imposing the energy constraint raises the requirement further, to 0.4 to 0.6 km^3 of ice under the mass-proportional partition.

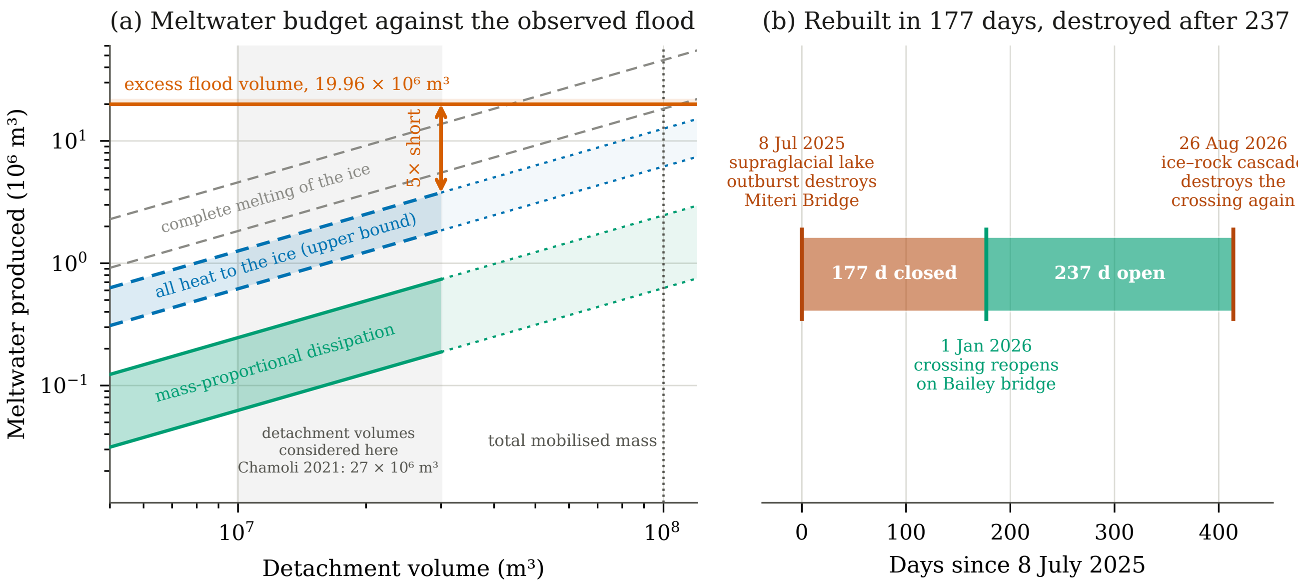

Figure 4. Water source and reconstruction cycle. (a) Meltwater produced by frictional dissipation against detachment volume. The green band is the mass-proportional partition and the blue band the upper bound in which all frictional heat reaches the ice, each spanning ice fractions of 0.2 to 0.5, drops of 1200 to 1830 m and initial ice temperatures of 0 to $-5\,°C$. Both fade beyond 3×10^7 m^3, where the axis ceases to describe an ice-bearing detachment. Grey dashed lines show complete melting with no energy constraint, and the arrow marks the shortfall at the most favourable corner of the parameter space, where the upper bound still falls five-fold short of the observed flood volume shown in orange. (b) The Rasuwagadhi crossing between the two events, destroyed on 8 July 2025, reopened after 177 days and destroyed again after 237 days in operation.

The bound is conditional on the detached volume, and the condition is worth stating plainly. If the detached ice-bearing mass were as large as 10^8 m^3, the ceiling would rise to 31 to 63 % of the flood and frictional melt could not be excluded on these grounds. That figure is the total mobilised mass including entrained channel and valley fill, which contains no glacier ice, and a detachment of 10^8 m^3 at 30 % ice would imply 30×10^6 m^3 of glacier ice leaving a single face, larger than the whole Chamoli detachment. Resolving this requires differencing the source-area topography, which the open imagery record does not currently permit. That measurement is the decisive test of the melt hypothesis and is stated here as a falsifiable prediction.

Within the adopted volume range, at least 80 % of the flood water, and more plausibly over 95 %, was not frictional meltwater. It was pre-existing channel water at monsoon stage, pore water in entrained saturated sediment, and water impounded behind the blockage and released on its failure. Available data do not constrain the partition among these three, though the 12.8 min transit to Syabrubesi limits the impoundment-and-breach interval to the order of minutes, which argues that the impounded share was modest. The event is an avalanche-induced channel blockage and breach, in the lineage of Sedongpu (Li et al., 2022) and the rockfall-triggered outburst at Barun (Byers et al., 2019). For reference, the potential energy of 10 to 30×10^6 m^3 falling 1200 to 1830 m at a bulk density of 2000 kg m^{-3} is 2.4×10^{14} to 1.1×10^{15} J, equivalent to M 6.4 to 6.8 if fully radiated seismically, against an observed M 5.2. Only a small fraction of that energy reaches the seismic wavefield, so magnitude alone underestimates mass, which is part of why the trigger was first logged as a moderate earthquake. Once a detachment is detected, the quantity that governs downstream consequence is the blockage and its impoundment. A minutes-scale breach favours a transient, permeable blockage that overtopped and incised rapidly over a sustained landslide dam, and that is a falsifiable statement. An independent hydraulic reconstruction has since routed the alternative and found that a sustained dam and breach reaches the border half an hour to an hour late and peaks near a third of the measured trimline heights, while a blockage failing within minutes and a direct debris flow both remain admissible (geo-pera, 2026). The residual blockage subsequently impounded a barrier lake in Gyirong County, China, that reached about 2×10^6 m^3 and an overtopping state within 24 h, prompting a Level-IV alert and suspension of rescue operations on both sides of the border.

3.5 Reconstruction cycle against hazard recurrence

This corridor was destroyed 414 days earlier. On 8 July 2025 an outburst from a previously uncatalogued supraglacial lake at about 5150 m on the Chinese side of the border, some 36 km upstream of Rasuwagadhi, destroyed the Miteri Sino-Nepal Friendship Bridge and the Rasuwagadhi dry port and damaged seven hydropower projects. The lake had grown from a small pond in December 2023 or 2024 to 0.64 to 0.75 km^2 by June 2025, according to the joint DHM and ICIMOD assessment. The border closed for 177 days at a reported cost exceeding NPR 22 bn in lost import revenue, and reopened on 1 January 2026 on a 91 m Bailey bridge built with Chinese support, then operated for 237 days (Fig. 4b). The 2026 event damaged 14 hydropower projects totalling about 748 MW and destroyed 40 to 42 km of the only overland road connecting Kathmandu to the Chinese border at Rasuwagadhi, which is the kind of concentrated exposure that Schwanghart et al. (2016) quantified for Himalayan hydropower against outburst floods. Damage figures are provisional press reports from the days immediately after the event. The same 40 km of valley was therefore struck twice by physically independent cryospheric mechanisms, first supraglacial lake drainage and then bedrock–ice detachment with channel blockage and breach.

The regional context requires the disambiguation noted in Sect. 2. The frequently cited outburst record of 1935, 1964 and 1981, and the 2016 Gongbatongshacuo event that Cook et al. (2018) showed to be measurable as a driver of fluvial erosion, all belong to the Poiqu basin, which drains to the other Bhote Koshi and thence to the Sun Koshi at Kodari, about 68 km east of Rasuwagadhi and in a different river system. No documented outburst record exists for the Trishuli corridor before 2025, and absence of record is not absence of events, because this corridor was ungauged and lightly reported before the dry port was built. The two histories together support the regional argument that both transboundary Bhote Koshi corridors are outburst-prone, and they do not support a single-channel recurrence series.

Exposure in this corridor is partly a product of the previous disaster. The community described in Sect. 3.3 had been resettled on the low-lying banks of the Trishuli after the 2015 Gorkha earthquake, so post-disaster reconstruction placed those households on the active floodplain of a river whose upstream hazard was already documented. Return-period design is poorly suited to this setting, because it treats each mechanism separately and assumes stationarity, so it does not represent the joint cryospheric hazard at a point. The operational arithmetic is simpler, in that rebuilding took 177 of the 414 days between the two events, or 43 % of the interval, and the replacement crossing operated for 237 days before the second event destroyed it. The reconstruction was carried out quickly and under acute pressure to restore a trade route on which the district depends, and the design question it leaves is how to carry an interval this short into the next rebuild, alongside cost and lead time.

4 Discussion

The results converge on one design conclusion, and the downstream hydrology sharpens it. DHM assessed the Devghat stage as corresponding to a 2 to 3 year return period, a stage-based agency assessment adopted here as such and not independently verified. By the time the wave had travelled 190 km it was, in conventional flood-frequency terms, an ordinary event, and it never crossed the Devghat warning threshold. The lethal zone was defined by the reach in which no warning could physically arrive, so magnitude does not explain the mortality pattern while lead time does. That inference has a limit worth stating. Along a single flow path, lead time and flow intensity are collinear, because the near field had both the shortest warning and a hyperconcentrated debris flow at 38 m s^{-1}, while the far field had hours of warning and an ordinary flood wave. Near-field mortality may therefore have been intensity-limited as well as warning-limited, and this design cannot separate the two. The failure occurred at 08:37 in daylight, which is favourable for evacuation and makes the absence of warning, and not the impossibility of response, the operative constraint, and exposure was concentrated by the resettlement described in Sect. 3.5 in precisely the reach with no lead time. Neither consideration resolves the collinearity, which a per-reach exposure normalisation would address once population and building data at that scale are available.

Nepal's current architecture rests on downstream gauges and on a manual escalation path. The event destroyed three of those gauges within the first 43 minutes and two never crossed a threshold. Three changes follow, in priority order. The most important is automated source-side seismic triggering, meaning continuous discrimination of surface-source signals in the glacierised headwaters, wired to public dissemination without a human relay. It is the only architecture tested here that places the first inhabited settlement on the positive side of zero, it exploits a detection capability already demonstrated at this range by Cook et al. (2021), and because the source lies inside Nepal it requires no cross-border agreement. The second change is to treat telemetry loss as an alarm condition in its own right, as Sect. 3.2 sets out. It costs nothing, and it would have advanced domestic detection by about ten minutes. The third change is machine-to-machine notification for the blockage and the barrier lake, which formed on the Chinese side of the border and are the specific hazard that such notification would address. Where no achievable warning latency helps, as at Timure and Rasuwagadhi, the available instruments are land-use restriction, elevated alignment for critical crossings, and a decision not to rebuild the same assets on the same terraces.

Pre-failure deformation monitoring would not have solved the timing problem. At Chamoli, optical feature tracking resolved 20 to 30 m of horizontal pre-collapse displacement over roughly the five years before failure, concentrated in summer, and the same study states that the timing of collapse could not have been forecast from satellite data alone (van Wyk de Vries et al., 2022). Systematic screening of Himalayan slopes on this basis is nonetheless feasible and overdue (Ahmed et al., 2026). Susceptibility and timing are different problems, because interferometry and feature tracking can identify which slopes above which settlements deserve instrumentation and land-use attention, and could not have identified 26 August as the day. That is why the post-failure lead-time budget is the operative quantity.

A further observation concerns the evidence base itself. Three days after the event, Nepal's machine-readable disaster database carried eight flood incidents for the affected corridor whose linked loss records totalled zero deaths and zero missing, and no event record had yet been opened for the cascade. Every casualty figure in circulation, including those used here, therefore traces to situation reports and press releases, not to the structured portal. This is a predictable consequence of load, because the same staff who would populate the database were conducting the response, and the portal depends on the same manual reporting path as the warning chain. Both are limited by that path, which is an argument for automating the entry of agency-issued figures rather than a criticism of the agencies compiling them. The record here documents the state of the portal on 29 August 2026, and it may since have been backfilled.

The same corridor produced two floods in 414 days from mechanisms that current inventories treat as unrelated. Glacial lake inventories (Veh et al., 2020; Shugar et al., 2020; Taylor et al., 2023) would not have flagged an ice–rock detachment, and detachment inventories (Kääb et al., 2021) would not have flagged a supraglacial pond that formed within eighteen months. Corridors such as this one require joint cryospheric hazard assessment at reach scale, integrating lake growth, slope stability and blockage potential. Haeberli et al. (2017) made the same argument for de-glaciating ranges where degrading permafrost creates new lakes and destabilises the slopes above them, and the multihazard framing after Melamchi 2021 called for it as well (Maharjan et al., 2021; Kargel et al., 2016). The boundary condition is the state of the catchment itself. Langtang has lost 41.5 % of its glacier area since the Little Ice Age, its rate of loss has more than quadrupled, and warming there is elevation-dependent, running at about 0.3 °C decade^{-1} above 4000 m against 0.1 °C decade^{-1} lower down (Silwal et al., 2026). That gradient concentrates change on exactly the elevations where these failures begin, and the same deglaciation is projected to raise outburst risk across the Third Pole (Zheng et al., 2021).

5 Limitations

Several analyses that would strengthen this work are not yet supportable, so they are excluded here. No hydrodynamic simulation is offered, because there is no calibrated digital elevation model, no measured inflow hydrograph and no field validation, so any depth or velocity field would be uncalibrated. Reconstructing the cascade properly would require the sequence of source-volume, two-phase runout and hydrodynamic models that Lala et al. (2018) applied to an outburst process chain elsewhere in the Nepal Himalaya, with a solver able to carry the solid and fluid phases together (Mergili et al., 2017), and the inputs that sequence needs do not yet exist for this event. No detachment volume is estimated either, and the open imagery record explains why. Two independent releases cover the event, of thirteen and twenty-four very-high-resolution scenes (Vantor, 2026; Planet Labs PBC, 2026), reaching 0.55 m and including an acquisition three hours after the failure, so neither resolution nor latency is the deficiency. Neither carries stereo pairs or elevation products. The source is imaged twice after the event, at 3.4 and 3.8 m under 81 to 88 % cloud, and never before it, so no before-and-after pair exists there and the scar geometry cannot be differenced. The most recent open pre-event scene containing Syabrubesi predates the failure by three months.

The timing data carry more uncertainty than their reported precision suggests. The chronology is minute-resolution, gauge nodes are bracketed only within their reporting cycle, and the Mugling entry is logged as confirmed-past and is therefore an upper bound on front arrival. These are propagated into the celerity ranges and the lead-time brackets, and they are the reason the counterfactual gain at Syabrubesi is reported as a range and not as a single value. The mortality-location claim rests on inference rather than on a census, as Sect. 3.3 sets out, and the collinearity of lead time with flow intensity along a single corridor is not resolved by this design. No formal attribution is offered either, and the documented warming and destabilisation context is reported without asserting a fraction of attributable risk. No antecedent-meteorology claim is made either, because circulating accounts of a preceding warm spell are not yet supported by gauge or reanalysis evidence. Casualty figures remain provisional, and the analysis uses only their spatial distribution, which is stable across revisions, together with aggregate counts.

6 Conclusions

The mass public alert followed the physical trigger by 38.8 minutes while the wave reached the first inhabited gauge in 12.8 minutes, giving a lead time of -26 min at Syabrubesi and between -6 and $+4$ min at Betrawati. Reported fatalities concentrated in those two districts, while districts warned hours in advance became the body-recovery zone. The two uppermost destroyed gauges were lost at 27 % and 87 % of their own warning stages, so threshold logic never fired, and the only signal that did travel at the speed of the event, the simultaneous loss of telemetry, is still classified as an equipment fault. Automated source-side seismic detection with a five-minute budget to public message would have delivered between -2 and $+8$ min at Syabrubesi instead of -26 min, and about 34 additional minutes at every settlement below Betrawati. Because the detachment occurred inside Nepal, that measure requires no cross-border agreement.

Frictional melting of the detached ice cannot account for the flood. Supplying the 19.96×10^6 m^3 excess volume measured at Devghat would require complete melting of 21.8×10^6 m^3 of ice, four times the ice content of the entire Chamoli 2021 detachment. The water came from the channel and from impoundment behind a transient blockage, which relocates the post-detachment monitoring target from the glacier to the blockage. At Devghat the event corresponded to a 2 to 3 year return period on DHM's assessment and never crossed the station's warning threshold. Rebuilding the Rasuwagadhi crossing consumed 177 of the 414 days between two destructive events from independent cryospheric mechanisms, and the replacement operated for 237 days before it was destroyed. An interval this short belongs in the design case for the replacement asset, alongside its cost and lead time.

Code availability. The analysis that produces every figure and table in this paper is archived at 10.5281/zenodo.22153581 under CC-BY-4.0. It is written in Python and relies on NumPy (Harris et al., 2020) and Matplotlib (Hunter, 2007).

Data availability. The data package underlying every figure, table and number in this paper is archived at 10.5281/zenodo.22153581 under CC-BY-4.0. Each field in it carries its own source and evidence grade, so any value here can be traced to the record it came from. Five sources supply everything. Seismic origin times, locations, magnitudes and event classification come from the USGS Advanced National Seismic System Comprehensive Catalog (U.S. Geological Survey, 2026), and the event overview and runout distance from the USGS Landslide Hazards Program (USGS, 2026). The chronology, the official gauge thresholds, the discharge analysis and the flood volume come from the technical situation report issued on 26 August 2026 by the Flood Forecasting Division of Nepal's Department of Hydrology and Meteorology, for which no permanent public URL was located and which was obtained through contemporaneous reproductions whose quoted figures agree with one another, the copy used being archived with the data. The channel centreline, the international boundary and all settlement coordinates come from OpenStreetMap (OpenStreetMap contributors, 2026). Building damage comes from the grading products of Copernicus Emergency Management Service activation EMSR927 (Copernicus Emergency Management Service, 2026), and casualty and recovery figures from NDRRMA and Nepal Police situation reports of 28 and 29 August 2026. Personal data of disaster victims were deliberately excluded. Named missing-person registries and hospital and rescue manifests that were publicly reachable during the response were not ingested, and only aggregate counts appear anywhere in the archive.

Author contributions. The sole author was responsible for conceptualisation, data curation, formal analysis, investigation, methodology, software, validation, visualisation, and writing of the original draft and its revision. Contributions are described using the CRediT taxonomy. No funding was acquired, and no supervision, project administration or provision of resources by others applies to this work.

Competing interests. The author declares that there is no conflict of interest.

Acknowledgements. The Department of Hydrology and Meteorology and NDRRMA of Nepal released operational chronologies during an active emergency, ICIMOD provided rapid technical assessment, and the USGS Landslide Hazards and Earthquake Hazards Programs and the Copernicus Emergency Management Service released data openly and immediately. The maintainers of OpenStreetMap are gratefully acknowledged. This paper records the loss of the four hydrological stations destroyed in this event, and of the personnel and communities of the Bhote Koshi–Trishuli corridor.

Financial support. This research received no external funding.

References

Ahmed, R., Bhardwaj, A., Sam, L., and Van Tricht, L.: Ice-rock avalanches in a warming Himalaya indicate pathways toward effective preparedness, Communications Earth & Environment, 7, 217, https://doi.org/10.1038/s43247-026-03352-y, 2026.

Badoux, A., Graf, C., Rhyner, J., Kuntner, R., and McArdell, B. W.: A debris-flow alarm system for the Alpine Illgraben catchment: design and performance, Natural Hazards, 49, 517–539, https://doi.org/10.1007/s11069-008-9303-x, 2009.

Byers, A. C., Rounce, D. R., Shugar, D. H., Lala, J. M., Byers, E. A., and Regmi, D.: A rockfall-induced glacial lake outburst flood, Upper Barun Valley, Nepal, Landslides, 16, 533–549, https://doi.org/10.1007/s10346-018-1079-9, 2019.

Cook, K. L., Andermann, C., Gimbert, F., Adhikari, B. R., and Hovius, N.: Glacial lake outburst floods as drivers of fluvial erosion in the Himalaya, Science, 362, 53–57, https://doi.org/10.1126/science.aat4981, 2018.

Cook, K. L., Rekapalli, R., Dietze, M., Pilz, M., Cesca, S., Rao, N. P., Srinagesh, D., Paul, H., Metz, M., Mandal, P., Suresh, G., Cotton, F., Tiwari, V. M., and Hovius, N.: Detection and potential early warning of catastrophic flow events with regional seismic networks, Science, 374, 87–92, https://doi.org/10.1126/science.abj1227, 2021.

Copernicus Emergency Management Service: EMSR927: Flood in Nepal, grading products for Syapru Besi, Timure and Bidur, European Commission, Joint Research Centre, Copernicus EMS Rapid Mapping, https://mapping.emergency.copernicus.eu/activations/EMSR927/, last access: 29 August 2026, 2026.

Ekström, G. and Stark, C. P.: Simple scaling of catastrophic landslide dynamics, Science, 339, 1416–1419, https://doi.org/10.1126/science.1232887, 2013.

Fujita, K., Inoue, H., Izumi, T., Yamaguchi, S., Sadakane, A., Sunako, S., Nishimura, K., Immerzeel, W. W., Shea, J. M., Kayastha, R. B., Sawagaki, T., Breashears, D. F., Yagi, H., and Sakai, A.: Anomalous winter-snow-amplified earthquake-induced disaster of the 2015 Langtang avalanche in Nepal, Natural Hazards and Earth System Sciences, 17, 749–764, https://doi.org/10.5194/nhess-17-749-2017, 2017.

geo-pera: Reconstruction of the 26 August 2026 Bhote Koshi outburst flood from open satellite data, Rapid reconstruction, code under MIT licence, https://github.com/geo-pera/bhotekoshi-2026-reconstruction, last access: 29 August 2026, 2026.

GFZ Helmholtz Centre for Geosciences: GEOFON event `gfz2026qrfy`: Nepal–China border region (landslide), GEOFON Program, GFZ Helmholtz Centre for Geosciences, Potsdam, https://geofon.gfz.de/eqinfo/event.php?id=gfz2026qrfy, last access: 29 August 2026, 2026.

Gruber, S. and Haeberli, W.: Permafrost in steep bedrock slopes and its temperature-related destabilization following climate change, Journal of Geophysical Research: Earth Surface, 112, F02S18, https://doi.org/10.1029/2006JF000547, 2007.

Haeberli, W., Schaub, Y., and Huggel, C.: Increasing risks related to landslides from degrading permafrost into new lakes in de-glaciating mountain ranges, Geomorphology, 293, 405–417, https://doi.org/10.1016/j.geomorph.2016.02.009, 2017.

Harris, C. R., Millman, K. J., van der Walt, S. J., Gommers, R., Virtanen, P., Cournapeau, D., Wieser, E., Taylor, J., Berg, S., Smith, N. J., Kern, R., Picus, M., Hoyer, S., van Kerkwijk, M. H., Brett, M., Haldane, A., del Río, J. F., Wiebe, M., Peterson, P., Gérard-Marchant, P., Sheppard, K., Reddy, T., Weckesser, W., Abbasi, H., Gohlke, C., and Oliphant, T. E.: Array programming with NumPy, Nature, 585, 357–362, https://doi.org/10.1038/s41586-020-2649-2, 2020.

Hugonnet, R., McNabb, R., Berthier, E., Menounos, B., Nuth, C., Girod, L., Farinotti, D., Huss, M., Dussaillant, I., Brun, F., and Kääb, A.: Accelerated global glacier mass loss in the early twenty-first century, Nature, 592, 726–731, https://doi.org/10.1038/s41586-021-03436-z, 2021.

Humanitarian OpenStreetMap Team: Nepal flood 2026: flood affected area, Bhote Koshi and Trishuli, Humanitarian Data Exchange, Open Database License (ODbL), https://data.humdata.org/dataset/hot_flood_npl, last access: 29 August 2026, 2026.

Hunter, J. D.: Matplotlib: a 2D graphics environment, Computing in Science & Engineering, 9, 90–95, https://doi.org/10.1109/MCSE.2007.55, 2007.

ICIMOD: Major flash flood sweeps through Nepal's Rasuwa district, raising fears of further downstream flooding, Press release, International Centre for Integrated Mountain Development, Kathmandu, https://www.icimod.org/press-release/major-flash-flood-sweeps-through-nepals-rasuwa-district-raising-fears-of-further-downstream-flooding/, last access: 28 August 2026, 2026.

Immerzeel, W. W., Lutz, A. F., Andrade, M., Bahl, A., Biemans, H., Bolch, T., Hyde, S., Brumby, S., Davies, B. J., Elmore, A. C., Emmer, A., Feng, M., Fernández, A., Haritashya, U., Kargel, J. S., Koppes, M., Kraaijenbrink, P. D. A., Kulkarni, A. V., Mayewski, P. A., Nepal, S., Pacheco, P., Painter, T. H., Pellicciotti, F., Rajaram, H., Rupper, S., Sinisalo, A., Shrestha, A. B., Viviroli, D., Wada, Y., Xiao, C., Yao, T., and Baillie, J. E. M.: Importance and vulnerability of the world's water towers, Nature, 577, 364–369, https://doi.org/10.1038/s41586-019-1822-y, 2020.

Kääb, A., Leinss, S., Gilbert, A., Bühler, Y., Gascoin, S., Evans, S. G., Bartelt, P., Berthier, E., Brun, F., Chao, W.-A., Farinotti, D., Gimbert, F., Guo, W., Huggel, C., Kargel, J. S., Leonard, G. J., Tian, L., Treichler, D., and Yao, T.: Massive collapse of two glaciers in western Tibet in 2016 after surge-like instability, Nature Geoscience, 11, 114–120, https://doi.org/10.1038/s41561-017-0039-7, 2018.

Kääb, A., Jacquemart, M., Gilbert, A., Leinss, S., Girod, L., Huggel, C., Falaschi, D., Ugalde, F., Petrakov, D., Chernomorets, S., Dokukin, M., Paul, F., Gascoin, S., Berthier, E., and Kargel, J. S.: Sudden large-volume detachments of low-angle mountain glaciers, more frequent than thought?, The Cryosphere, 15, 1751–1785, https://doi.org/10.5194/tc-15-1751-2021, 2021.

Kargel, J. S., Leonard, G. J., Shugar, D. H., Haritashya, U. K., Bevington, A., Fielding, E. J., Fujita, K., Geertsema, M., Miles, E. S., Steiner, J., Anderson, E., Bajracharya, S., Bawden, G. W., Breashears, D. F., Byers, A., Collins, B., Dhital, M. R., Donnellan, A., Evans, T. L., Geai, M. L., Glasscoe, M. T., Green, D., Gurung, D. R., Heijenk, R., Hilborn, A., Hudnut, K., Huyck, C., Immerzeel, W. W., Liming, J., Jibson, R., Kääb, A., Khanal, N. R., Kirschbaum, D., Kraaijenbrink, P. D. A., Lamsal, D., Shiyin, L., Mingyang, L., McKinney, D., Nahirnick, N. K., Zhuotong, N., Ojha, S., Olsenholler, J., Painter, T. H., Pleasants, M., Pratima, K. C., Yuan, Q. I., Raup, B. H., Regmi, D., Rounce, D. R., Sakai, A., Donghui, S., Shea, J. M., Shrestha, A. B., Shukla, A., Stumm, D., van der Kooij, M., Voss, K., Xin, W., Weihs, B., Wolfe, D., Lizong, W., Xiaojun, Y., Yoder, M. R., and Young, N.: Geomorphic and geologic controls of geohazards induced by Nepal's 2015 Gorkha earthquake, Science, 351, aac8353, https://doi.org/10.1126/science.aac8353, 2016.

Lala, J. M., Rounce, D. R., and McKinney, D. C.: Modeling the glacial lake outburst flood process chain in the Nepal Himalaya: reassessing Imja Tsho's hazard, Hydrology and Earth System Sciences, 22, 3721–3737, https://doi.org/10.5194/hess-22-3721-2018, 2018.

Li, W., Zhao, B., Xu, Q., Scaringi, G., Lu, H., and Huang, R.: More frequent glacier-rock avalanches in Sedongpu gully are blocking the Yarlung Zangbo River in eastern Tibet, Landslides, 19, 589–601, https://doi.org/10.1007/s10346-021-01798-z, 2022.

Maharjan, S. B., Steiner, J. F., Shrestha, A. B., Maharjan, A., Nepal, S., Shrestha, M. S., Bajracharya, B., Rasul, G., Shrestha, M., Jackson, M., and Gurung, S.: The Melamchi flood disaster: cascading hazard and the need for multihazard risk management, Tech. rep., ICIMOD, Kathmandu, https://doi.org/10.53055/icimod.981, 2021.

Maurer, J. M., Schaefer, J. M., Rupper, S., and Corley, A.: Acceleration of ice loss across the Himalayas over the past 40 years, Science Advances, 5, eaav7266, https://doi.org/10.1126/sciadv.aav7266, 2019.

Mergili, M., Fischer, J.-T., Krenn, J., and Pudasaini, S. P.: r.avaflow v1, an advanced open-source computational framework for the propagation and interaction of two-phase mass flows, Geoscientific Model Development, 10, 553–569, https://doi.org/10.5194/gmd-10-553-2017, 2017.

OpenStreetMap contributors: Planet dump retrieved from https://planet.openstreetmap.org, Open Database License (ODbL); river centreline, international boundary and settlement data retrieved through the Overpass API, https://www.openstreetmap.org, last access: 28 August 2026, 2026.

Planet Labs PBC: Planet crisis response: Bhote Koshi–Trishuli outburst flood, Nepal, 2026, Source Cooperative, Creative Commons Attribution-NonCommercial 4.0, https://source.coop/planet/disasterdata/nepal-flash-flood-2026-08-26, last access: 29 August 2026, 2026.

Sättele, M., Bründl, M., and Straub, D.: Reliability and effectiveness of early warning systems for natural hazards: concept and application to debris flow warning, Reliability Engineering & System Safety, 142, 192–202, https://doi.org/10.1016/j.ress.2015.05.003, 2015.

Schwanghart, W., Worni, R., Huggel, C., Stoffel, M., and Korup, O.: Uncertainty in the Himalayan energy–water nexus: estimating regional exposure to glacial lake outburst floods, Environmental Research Letters, 11, 074 005, https://doi.org/10.1088/1748-9326/11/7/074005, 2016.

Shugar, D. H., Burr, A., Haritashya, U. K., Kargel, J. S., Watson, C. S., Kennedy, M. C., Bevington, A. R., Betts, R. A., Harrison, S., and Strattman, K.: Rapid worldwide growth of glacial lakes since 1990, Nature Climate Change, 10, 939–945, https://doi.org/10.1038/s41558-020-0855-4, 2020.

Shugar, D. H., Jacquemart, M., Shean, D., Bhushan, S., Upadhyay, K., Sattar, A., Schwanghart, W., McBride, S., van Wyk de Vries, M., Mergili, M., Emmer, A., Deschamps-Berger, C., McDonnell, M., Bhambri, R., Allen, S., Berthier, E., Carrivick, J. L., Clague, J. J., Dokukin, M., Dunning, S. A., Frey, H., Gascoin, S., Haritashya, U. K., Huggel, C., Kääb, A., Kargel, J. S., Kavanaugh, J. L., Lacroix, P., Petley, D., Rupper, S., Azam, M. F., Cook, S. J., Dimri, A. P., Eriksson, M., Farinotti, D., Fiddes, J., Gnyawali, K. R., Harrison, S., Jha, M., Koppes, M., Kumar, A., Leinss, S., Majeed, U., Mal, S., Muhuri, A., Noetzli, J., Paul, F., Rashid, I., Sain, K., Steiner, J., Ugalde, F., Watson, C. S., and Westoby, M. J.: A massive rock and ice avalanche caused the 2021 disaster at Chamoli, Indian Himalaya, Science, 373, 300–306, https://doi.org/10.1126/science.abh4455, 2021.

Silwal, G., Davies, B., Carr, J. R., King, O., Buzzard, S., Carrivick, J. L., and Baral, P.: Glacier changes in Langtang Catchment, Central Nepalese Himalaya from the Little Ice Age (~1815 CE) to 2023 CE, Global and Planetary Change, 264, 105 555, https://doi.org/10.1016/j.gloplacha.2026.105555, 2026.

Taylor, C., Robinson, T. R., Dunning, S., Carr, J. R., and Westoby, M.: Glacial lake outburst floods threaten millions globally, Nature Communications, 14, 487, https://doi.org/10.1038/s41467-023-36033-x, 2023.

U.S. Geological Survey: Advanced National Seismic System (ANSS) Comprehensive Catalog of earthquake events and products, U.S. Geological Survey Earthquake Hazards Program [data set], events `us7000tbwb` and `us7000tc90`, retrieved through the FDSN event web service, https://doi.org/10.5066/F7MS3QZH, https://earthquake.usgs.gov/earthquakes/search/, last access: 28 August 2026, 2026.

USGS: 2026 Nepal debris avalanche and flash flood, Landslide Hazards Program, U.S. Geological Survey, https://www.usgs.gov/programs/landslide-hazards/science/2026-nepal-debris-avalanche-and-flash-flood, last access: 28 August 2026, 2026.

van Wyk de Vries, M., Bhushan, S., Jacquemart, M., Deschamps-Berger, C., Berthier, E., Gascoin, S., Shean, D. E., Shugar, D. H., and Kääb, A.: Pre-collapse motion of the February 2021 Chamoli rock–ice avalanche, Indian Himalaya, Natural Hazards and Earth System Sciences, 22, 3309–3327, https://doi.org/10.5194/nhess-22-3309-2022, 2022.

Vantor: Open data: Nepal flooding, August 2026, Vantor (formerly Maxar) Open Data Program, Creative Commons Attribution-NonCommercial 4.0, https://vantor-opendata.s3.amazonaws.com/events/Nepal-Flooding-Aug-2026/collection.json, last access: 29 August 2026, 2026.

Veh, G., Korup, O., and Walz, A.: Hazard from Himalayan glacier lake outburst floods, Proceedings of the National Academy of Sciences of the United States of America, 117, 907–912, https://doi.org/10.1073/pnas.1914898117, 2020.

Zheng, G., Allen, S. K., Bao, A., Ballesteros-Cánovas, J. A., Huss, M., Zhang, G., Li, J., Yuan, Y., Jiang, L., Yu, T., Chen, W., and Stoffel, M.: Increasing risk of glacial lake outburst floods from future Third Pole deglaciation, Nature Climate Change, 11, 411–417, https://doi.org/10.1038/s41558-021-01028-3, 2021.